IEEE Access
Multidisciplinary | Rapid Review | Open Access Journal

Received 14 October 2022, accepted 15 November 2022, date of publication 28 November 2022,
date of current version 5 December 2022.

Digital Object Identifier 10.1109/ACCESS.2022.3225446

RESEARCH ARTICLE

Design and Characterization of 10-Elements MIMO Antenna With Improved Isolation and Radiation Characteristics for mm-Wave 5G Applications

SANJUKTA NEJ[1], ANUMOY GHOSH[1], SAROSH AHMAD[2,3], (Graduate Student Member, IEEE), JAYENDRA KUMAR[4], (Senior Member, IEEE), ADNAN GHAFFAR[5], AND MOUSA I. HUSSEIN[6], (Senior Member, IEEE)

[1]Department of Electronics and Communication Engineering, National Institute of Technology (NIT), Aizawl, Mizoram 796012, India
[2]Department of Signal Theory and Communications, Universidad Carlos III de Madrid, Leganés, 28911 Madrid, Spain
[3]Department of Electrical Engineering and Technology, Government College University Faisalabad (GCUF), Faisalabad 38000, Pakistan
[4]Department of Electronics Engineering, VIT-AP University, Amaravati, Andhra Pradesh, 522237, India
[5]Department of Electrical and Electronic Engineering, Auckland University of Technology, Auckland 1010, New Zealand
[6]Department of Electrical Engineering, United Arab Emirates University, Al Ain, United Arab Emirates

Corresponding authors: Sarosh Ahmad (saroshahmad@ieee.org) and Mousa I. Hussein (mihussein@uaeu.ac.ae)

ABSTRACT A ten-elements MIMO antenna with improved isolation and reduction of X-polar radiation (XPR) in millimeter (mm) wave region of n258 (24.25-27.5 GHz) is presented. The individual antenna element consists of stub loaded coplanar waveguide (CPW) structure with elliptical shaped radiator. Elliptical shaped Defected ground structure (DGS) has been incorporated at ground to reduce the mutual coupling effect between the adjacent antenna pairs and the minimum isolation obtained 35 dB. The backside of the substrate has a metallic plane with defects which is not connected to the coplanar ground of the antenna and it acts as a reflector to improve the radiation characteristics by lowering of XPR as well as improving the co-pol to X-pol isolation up to 20 dB and 28 dB in the boresight direction in both the XZ and YZ planes respectively. The diversity performances in terms of Envelope Correlation Coefficient (ECC), Diversity Gain (DG) and Channel Capacity Loss (CCL) are obtained as 0.1×10^{-6}, 10 dB and 0.005 bps/Hz respectively which are within the acceptable limits. Mean effective gain (MEG) values with respect to the excited port 2 and port 3 is identical and approximately -3 dB and the multiplexing efficiency of the proposed MIMO antenna is satisfactory over the bandwidth. The group delay is investigated and found to be almost constant with a variation of 1.2 ns thus indicating linear phase characteristic of the antenna. The proposed structure is compared with other mm-wave MIMO antennas and found to be advantageous. A prototype of the proposed 10-elements MIMO is fabricated, and the measured results resemble with the simulated results.

INDEX TERMS mm-wave MIMO, DGS, mutual coupling reduction, co-pol to X-pol isolation, DMS.

I. INTRODUCTION

mm-wave MIMO antenna is an essential component for MIMO systems for achieving a complete package of high data stream, multifunctional applications and future generation communication system with electrically compact layout [1]. Massive MIMO and beamforming techniques are inevitable to overcome the multipath losses and limited scattering in 5G mm-wave applications [2], [3]. 5th generation mobile network is a milestone in telecommunication industries in terms of data rate, connectivity, energy efficiency [4]. Next generation wireless communication is collaborating with different

The associate editor coordinating the review of this manuscript and approving it for publication was Mohammad Tariqul Islam.

industries such as vehicle radars, 5G smart remote devices, cellular and base station communication, wearable devices, etc. [5], [6], [7], [8]. In recent industries are expecting low profile transparent material to design smart devices that can be more convenient and applicable in portable flexible wearable devices [9]. Different countries already released licensed 5G frequency bands to exploit the mm-wave communication industries [10], [11], [12]. The basic 5G mm-wave licensed bands are n258 (24.25–27.50 GHz), n257 (26.5–29.5 GHz), n261 (27.50–28.35 GHz), n260 (37.0– 40.0 GHz), and n259 (39.5–43.5 GHz) [13].

The main drawback of a multiport wide band compact MIMO antenna system is high mutual coupling between antenna elements which influences the individual functionality of each antenna. The mutual coupling has been increased due the high surface current density induced for adjacent antenna elements which are placed near the excited port [14]. Different mutual decoupling mechanism have been discussed in different literature for microwave frequencies to reduce the mutual coupling such as incorporation of complementary rectangular spiral resonator and stub structure at the ground plane [15], [16], [17], parasitic microstrip line [18], DGS structure [14] and few literature investigated the mutual coupling reduction techniques for mm-wave frequencies as implementing metamaterial polarization-rotator wall [19], metasurface array including circular split ring-shaped cell [20] and incorporating split ring resonator [21].

Two complementary rectangular spiral resonators have been designed at the ground plane and a rectangular slot is engraved in between them to couple each other which act as an absorber. This structure effectively reduces mutual coupling between two antenna elements [15]. Two F-shaped stubs at the ground act as reflectors and enhances the isolation between the antenna pairs [16]. In [17], a rectangular stub has been designed along with ground plane which reduces the surface current between the antenna pairs that gradually decreases the mutual coupling. A line patch placed near the radiating elements at same side of the radiating patch blocks the extra current flow from the excited port to other port [18]. DGS structure has been incorporated by etching the ground plane and helps to minimize the surface current density between two antenna elements which effectively reduces the mutual coupling between the adjacent antennas and the position of the defect on the ground is very important to achieve the high isolation [14]. A metamaterial polarization-rotator wall has been placed in H-plane direction between two mm wave dielectric resonator antennas (DRAs) [19]. This wall rotates E-field by 90° which makes mutual coupling orthogonal that effectively decreases the mutual coupling between two DRAs. A different layer of metasurface array has been incorporated which cancels the near field coupling effect by transverse coupling current as the current at the two adjacent unit cells is in opposite direction and the coupled field between the antennas is distributed to the unit cells of the meta surface eventually decreasing the mutual coupling [20]. Similarly, in [21] an array of split ring resonator has been designed externally which prevents the leakage of the side wall radiation thus increasing the isolation level of two element MIMO [21]. Most of the literature implement different mutual coupling reduction techniques for dual elements MIMO. Few literatures reported mm wave MIMO with multilayered or 3D complex designs to overcome mutual coupling effects [19], [20], [21]. Furthermore, as antenna elements increase, the arrangement complexity as well as coupling effect also increases. It is evident that the complex multilayered structure is not practically implementable for sophisticated compact ten elements MIMO antenna.

High X-polar radiation (XPR) effect in high frequency application is very common. So, XPR suppression is essential to reduce crosstalk as well as it is beneficial for frequency reuse [14]. Generally, X-pol reduction technique has been discussed for single element antenna [22], [23], [24], [25], [26]. The methods include incorporation of DGS [22], [23], [24] for suppression of surface waves and shorted non radiating edge [25], [26]. The X-pol radiation has been induced due to presence of the strong orthogonal electric field whereas the defects on the ground plane weakens the orthogonal electric field. The circular shaped [22], dot and arc shaped [23], and elliptical shaped [24] defects are designed at the grounds for single patch antenna which reduces the X-polarization without major interference to the co polarization radiation for both E-plane and H-plane radiation characteristics. In [14], both mutual coupling and XPR reduction have been achieved by using DGS. Another strong reason for high X-polarization is high intensity of electric field existed at non-radiating edges. Therefore, shorting non radiating edges with ground [25] and shorting pins and extended stubs from the edges of the patch [26] are incorporated to reduce the electric field at the non-radiating edges of the single patch which effectively reduce the X-pol effects. Hybrid topology method has been introduced for 45° dual polarized closely space MIMO structure in [27] for XPR reduction. The Hybrid topology optimization method improves the X-polarization and radiation performances by enhancing the isolation between the pair of co-polarized ports and X-polarized ports. Mm-wave antenna with improvement of radiation characteristics have been reported by incorporating dual slots etching method for metasurface antenna [28], differential feeding techniques [29] and 180° out of phase arrangements of the array antenna elements [30]. In [28], a metasurface patch antenna includes four groups of coplanar patches where the coaxial probe is placed in the middle patch and excites the radiators. The X-polarization for H-plane has been deteriorated due to the middle patch that has been excited by the probe at the resonating frequency in the working band, therefore two slots have been etched out at the same patch which shifts the resonating frequency far away from the working band and overcome the problem. The differential feeding technique has been implemented by the rat race coupler mechanism which uses two feeding probes with equal amplitude and out of phase signal which diminishes the orthogonal fields eventually lowering the X-polarization [29]. The four port MIMO antenna

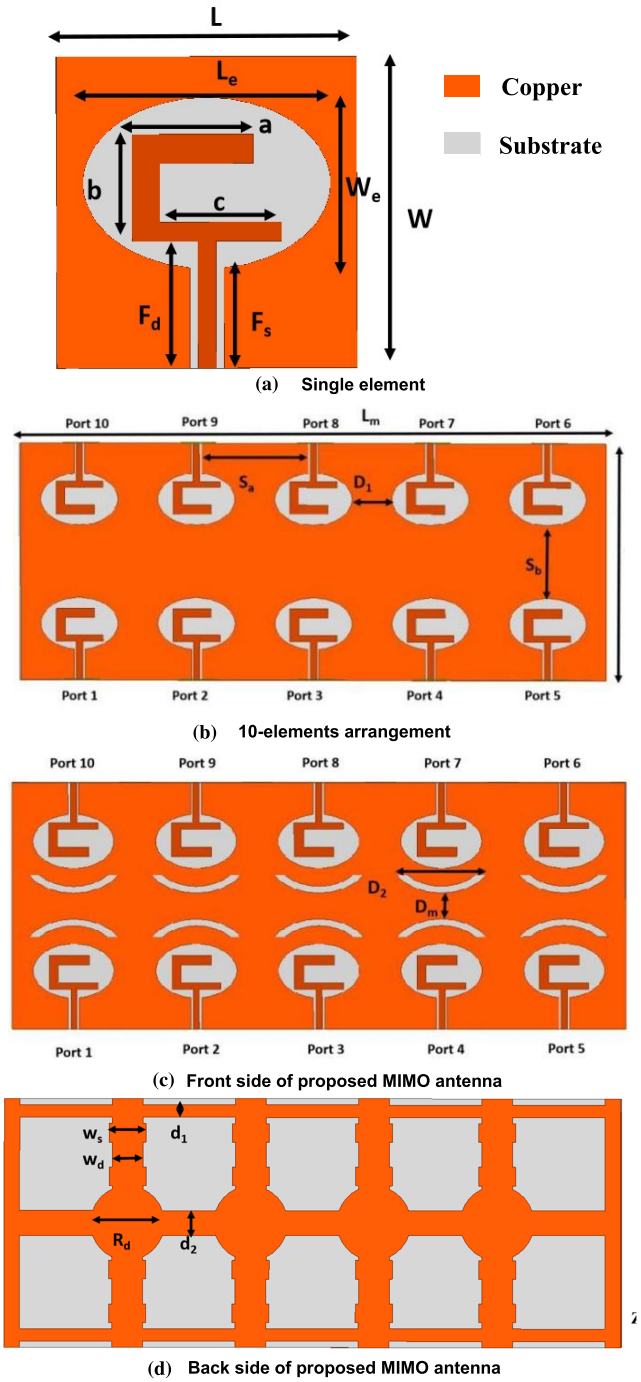

FIGURE 1. Schematic diagram of (a) single antenna, (b) 10-elements MIMO arrangement, (c) front view with DGS, and (d) back view with DMS.

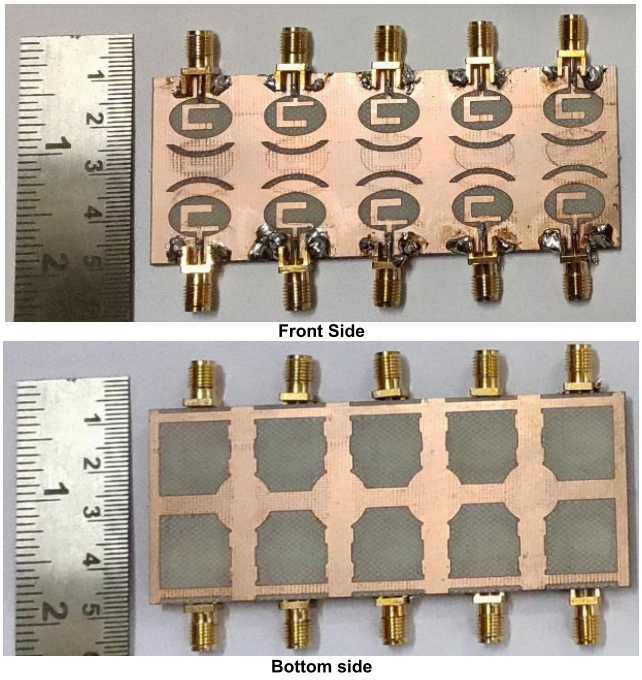

FIGURE 2. Photograph of fabricated 10-elements MIMO with DGS and DMS diagram.

includes array antennas as elements which are placed out of phase at side-by-side orientation that effectively suppresses the X-pol effect at the Ka band [30]. Most of the works of XPR reduction have been reported for either single antenna element, array antenna or 2-4 elements MIMO structures in microwave frequencies. Few designs are not limited to single layered system which become bulky as well as complicated. XPR reduction techniques for mm-wave MIMO antennas are extremely limited and it is a potential area of research yet to be explored fully.

In this article, a novel CPW-fed MIMO antenna has been designed which operates at mm-wave 5G band (n258) (24.25-27.5 GHz). Two techniques have been implemented to the proposed structure in terms of DGS and DMS structures for simultaneous reduction of mutual coupling and XPR in mm-wave region thereby substantially improving the |Sij| characteristic and co-pol to X-pol isolation radiation feature. The technique of mutual coupling has been exhibited by analyzing the simulated surface current density of the MIMO antenna with and without DGS structure. The XPR reduction have been analyzed by investigating the electric field distribution of the proposed structure after implementing the DMS structure. Improvement of scattering parameters and radiation characteristics of the proposed structure are presented by referring the design evolution of the MIMO structure. The MIMO functionality has been characterized through ECC, CCL, DG, MEG and multiplexing efficiency values. The group delay of the antenna elements has been investigated in far field region to understand the time domain behavior in the operating bandwidth. All the simulation pertaining to the proposed design have been executed using full wave simulation software HFSS v. 2021.

II. 10-ELEMENT MIMO ANTENNA CONFIGURATION

The single antenna design is based on CPW fed stub loaded configuration with elliptical shaped radiator with the stub having an asymmetric U-shaped structure as shown in Fig 1 (a). FR4 material with dielectric constant 4.4, loss tangent 0.02 and substrate height 1.6 mm has been chosen

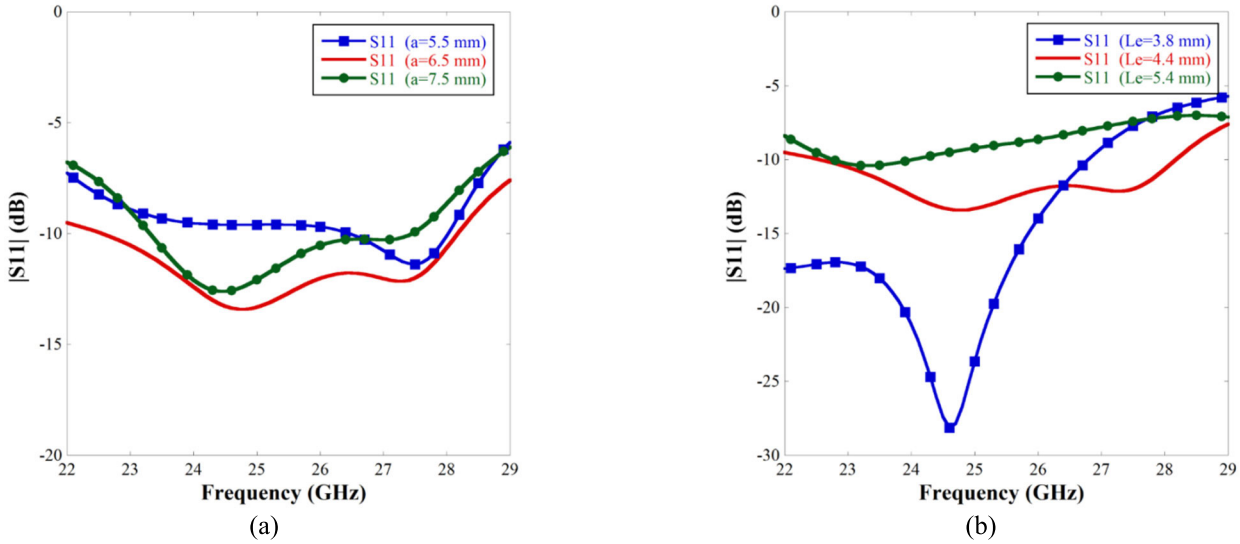

FIGURE 3. |S11| plot of the single antenna by varying (a) a, length of the stub and (b) L_e, length of the major axis of the elliptical radiator.

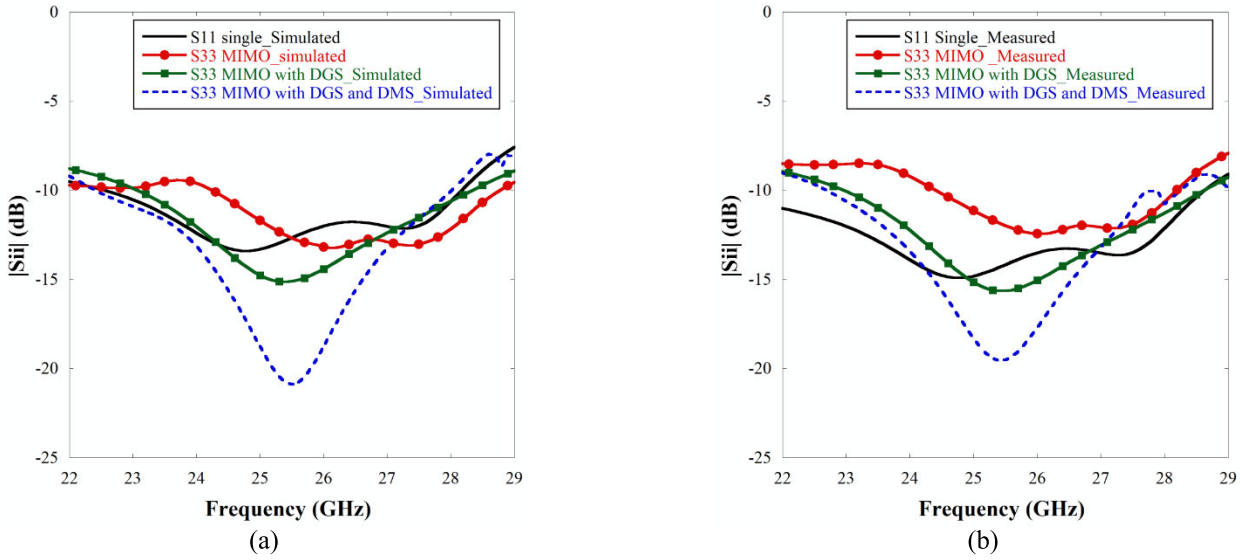

FIGURE 4. Comparison graph of (a) simulated and (b) measured |Sii| characteristics of the proposed structures.

as antenna substrate. The stub is designed to achieve the impedance matching over the desired operating bandwidth. The single antenna is extended to 10-elements MIMO configuration by placing the antenna elements in side-by-side and face-to-face orientation as depicted in Fig. 1 (b). Partial elliptical slots are engraved in the co-planar ground plane, as given in Fig. 1(c), to further reduce the mutual coupling. A metallic structure with defects is laminated at the backside of the substrate as illustrated in Fig. 1(d). It is to be observed that this defected metal layer does not form a part of the antenna ground. It acts as a reflector that reduces the XPR and enhances the co-pol to X-pol isolation without disturbing the S-parameters of the antenna shown in Fig. 1(d). The relevant dimensions pertaining to the antenna geometry are given in a Table 1. The final design of 10-elements MIMO with DGS and DMS has been fabricated and the photograph of the fabricated prototype is presented in Fig. 2. The measurement has been carried out by exciting one port while other ports are connected to 50-ohm matched load.

TABLE 1. Design parameters of proposed antenna.

Parameter	Dimension (mm)	Parameter	Dimension (mm)
L	16	W	16
L_m	100	Wm	40
a	6.5	D_1	5.2
b	5.5	D_2	15.7
c	7.5	D_m	4
L_e	14.8	d_1	3
W_e	8.9	d_2	5
F_d	6.5	W_d	4
F_s	5.5	W_s	4.3
S_a	18	R_d	10

TABLE 2. Comparison table between proposed work with existing work.

Ref.	mm-wave frequency (GHz)	Antenna elements	Inter element gap	Isolation (dB)	Min co-pol to X-pol isolation at boresight direction (dB)	ECC
[5]	25.1-37.5	4	0.49 λ	22	NP	<0.01
[6]	23.5-29.4	4	0.46 λ	20	NP	<0.004
[7]	27.4-28.5	4	0.56 λ	40	10	<0.0003
[8]	26.16–29.72	4	0.9 λ	30	NP	<0.0005
[9]	24.10 - 27.18 & 33 - 44.13	4	0.45 λ	16	15	<0.1
[10]	24.8–44.45	4	0.52 λ	20	10	<0.008
[12]	26.867-28.975	4	0.46 λ	18	NP	< 0:0013
[20]	24.55-26.5	4	0.52 λ	45	NP	$< 0.1X10^{-6}$
Proposed work	**22.5-28.5**	**10**	**0.44 λ**	**36.4**	**20**	$\mathbf{<0.1X10^{-6}}$

NP defined as not provided

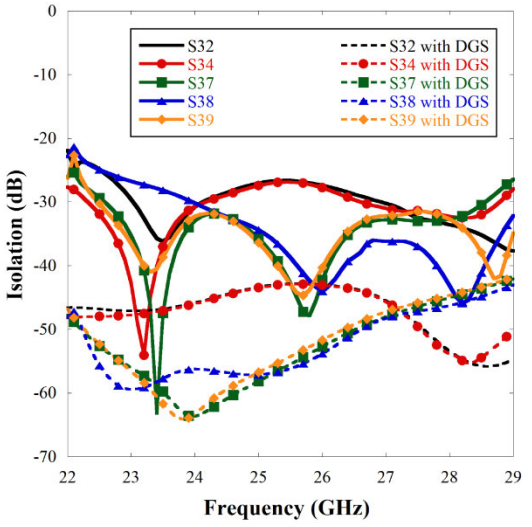

FIGURE 5. Isolation characteristics of the 10-elements MIMO antenna with and without DGS.

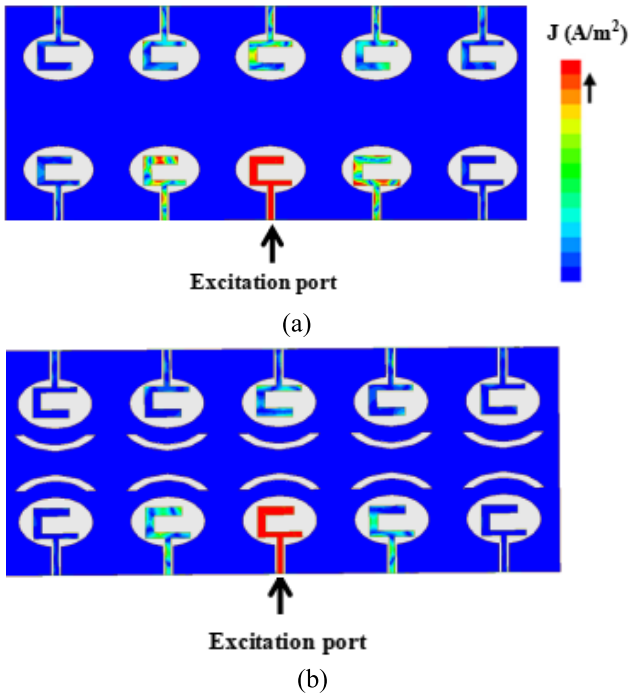

FIGURE 6. Current distribution plot of 10-elements MIMO antenna (a) without DGS and (b) with DGS.

III. RESULTS AND DISCUSSIONS

The single antenna consists of a stub and an elliptical radiator (refer to Fig. 1 (a)). The stub length is significant for resonating frequency as shown in Fig. 3 (a). From the figure it is observed that, the frequency has been shifted towards higher value while length is increasing and bandwidth also changing simultaneously. Similarly, the length of the major axis of the elliptical radiator is significant for wide bandwidth with frequency shift as presented in Fig. 3 (b). It is observed that the minor changes of the radiator dimension directly affect the bandwidth as well as frequency range.

Fig. 4(a) graphically compares the |Sii| characteristic of the antenna. It reveals that the operating bandwidth of the single element antenna (referring to Fig. 1(a)) is 24 % (22 GHz-28 GHz) When it is extended to 10-elements MIMO, the bandwidth becomes 18% (24.2 GHz-29 GHz). The impedance matching increases progressively on addition of DGS and DMS and the final proposed antenna has a bandwidth of 23.52% (22.5GHz-28.5 GHz) While simulating the MIMO antenna for |Sii| characteristic, port 3 is taken as the excitation port since it is at the middle of all the ports in one side. It has been verified that all other ports give almost the same |Sii| response. Fig. 4(b) gives the measured |Sii| responses for the proposed structures and it is observed that the measured results resemble with the simulated results in terms of bandwidth.

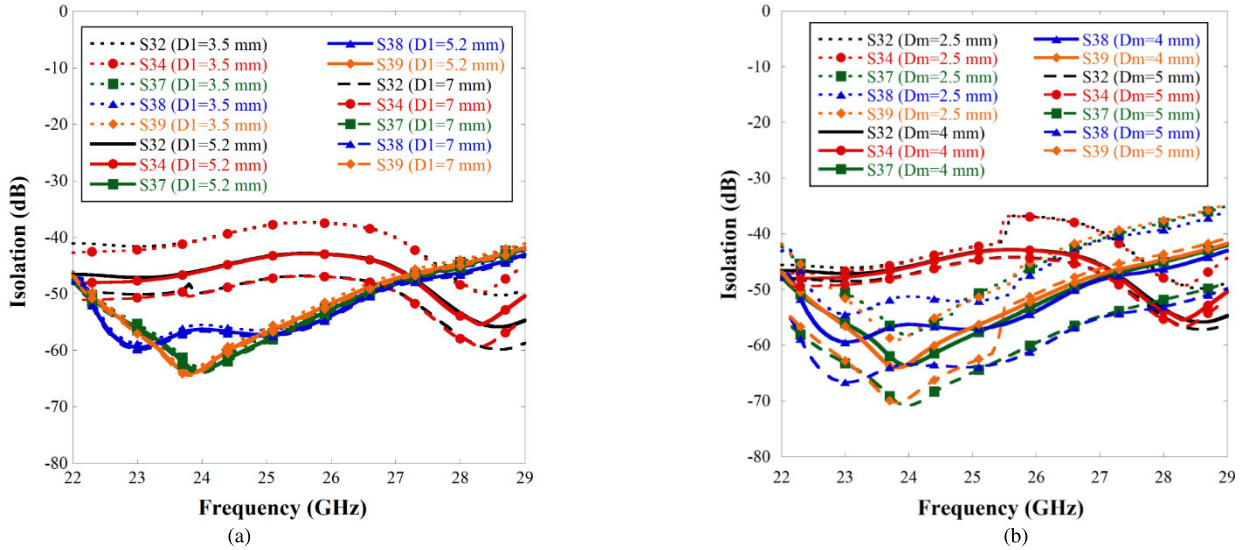

FIGURE 7. Isolation characteristics of the 10-elements MIMO antenna by varying the parameters (a) D_1 and (b) D_m.

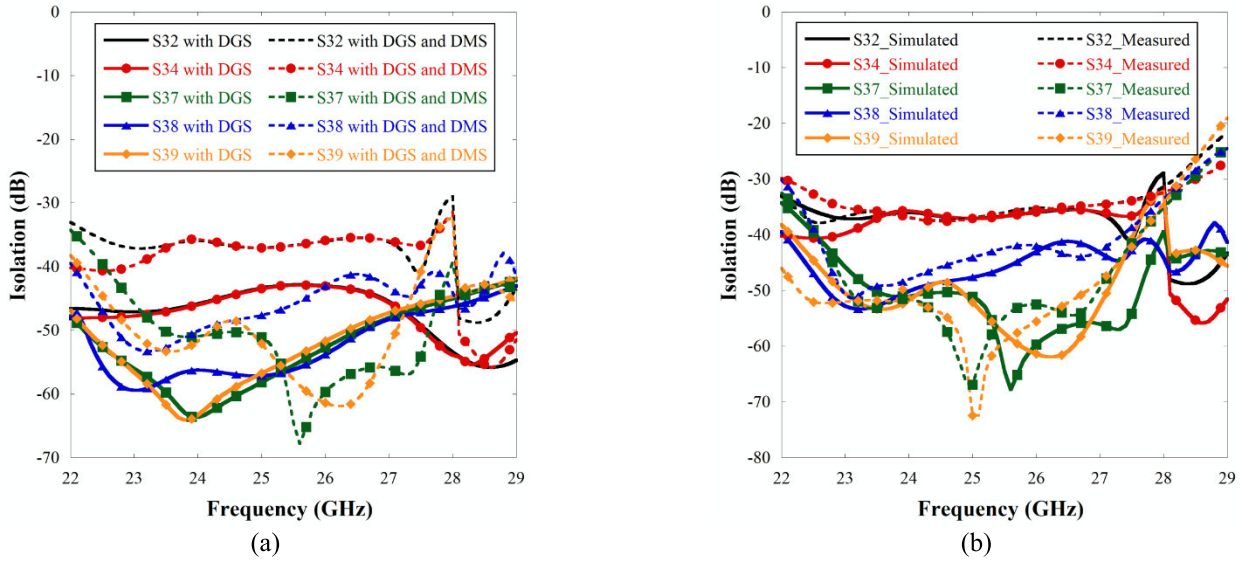

FIGURE 8. Isolation characteristics of (a) the 10-elements MIMO with DGS but without DMS and proposed structure with DGS and DMS, (b) simulated and measured results of proposed 10-elements MIMO with DGS and DMS.

A. ISOLATION IMPROVEMENT TECHNIQUE

Referring to Fig. 1(c), the excitation at the middle port (port 3) is considered to examine the mutual coupling effect for isolation improvement as it is surrounded by closely spaced antennas in all the possible orientations, that is, side-by-side (ports 2,3 and ports 3,4), face-to-face (3,8) and diagonal (3,7 and 3,9) thus effectively having more coupling compared to other ports. The isolation plot is presented in Fig. 5 for the MIMO antenna with and without DGS. It is perceived that the mutual coupling is significantly minimized by using the DGS structure and is below −40 dB within the operating bandwidth thereby indicating very high isolation between any pair of adjacent antenna elements. As expected, the highest coupling is observed for the adjacent antenna elements which are situated in side-by-side orientation although it is still below −40 dB. For the other orientations, the mutual coupling goes below −50 dB.

The simulated surface current density distribution of the 10-elements MIMO with and without DGS are given in Figs. 6(a) and 6(b) respectively. Fig. 6 (a) shows that while port 3 is excited, current is induced at the adjacent feedlines which subsequently makes the adjacent slots to radiate thereby inducing the effect of mutual coupling. The partial elliptical slots act as filters to suppress the surface waves. Hence, Fig. 6(b) indicates that on exciting port 3, almost negligible current is induced on the adjacent feedlines thereby decreasing the mutual coupling and improving the isolation. It is to be noted from Fig. 6(b) that the induced current density is slightly more in feedlines at ports 2 and 4 as compared to ports 7, 8, and 9. Therefore, the mutual coupling

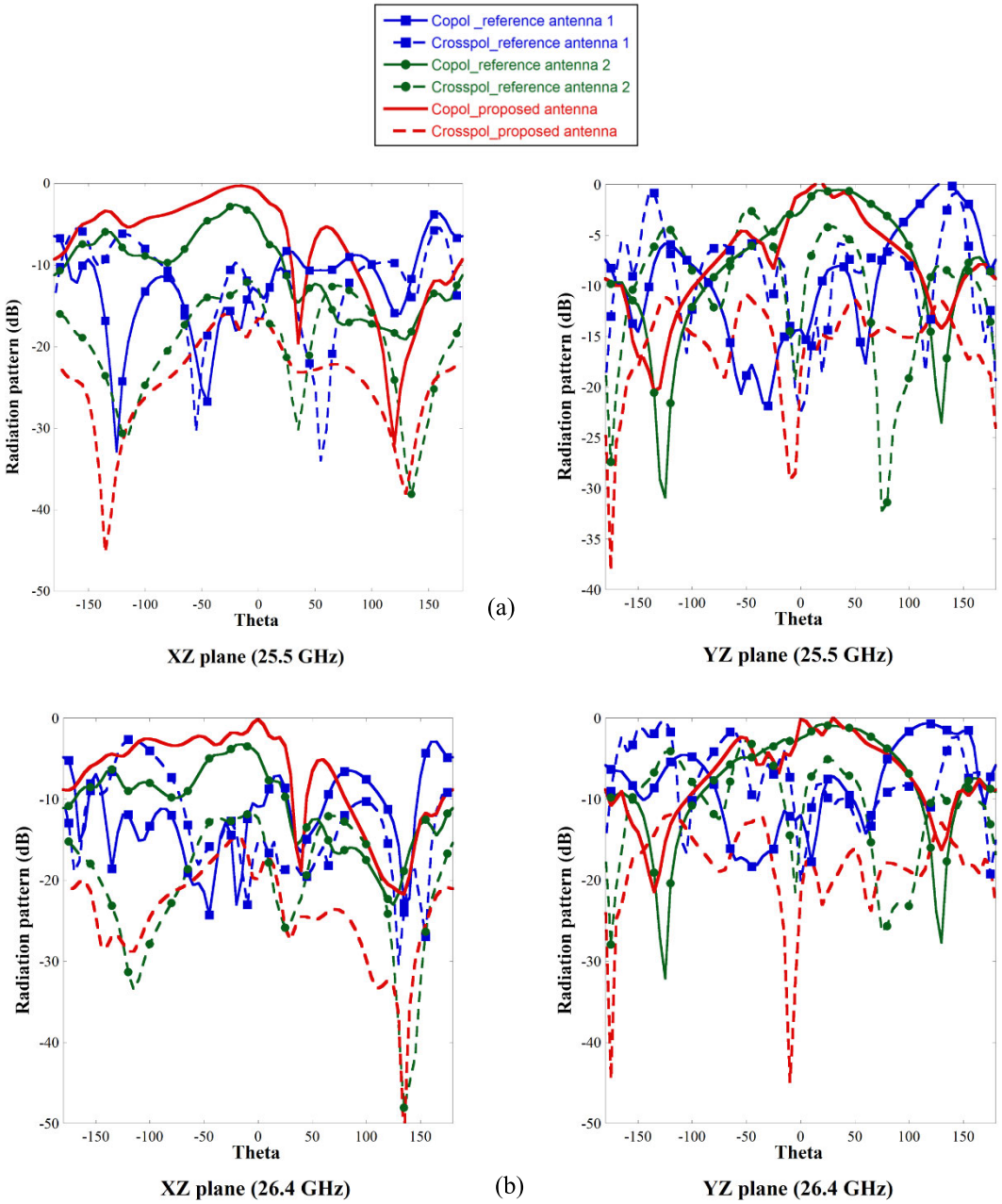

FIGURE 9. Comparison graph of XZ plane and YZ plane radiation pattern at (a) 25.5 GHz and (b) 26.4 GHz of 10-elements MIMO antenna without DGS and DMS (reference antenna), 10-elements MIMO antenna with DGS (reference antenna2) and 10-elements MIMO antenna with DGS and DMS (proposed antenna).

is more for side-by-side orientation than any other orientation as reflected in Fig. 5.

Referring to Figs. 1(b) and 1(c), the parameters D_1 and D_m are playing very vital roles affecting the isolation between the antenna elements. Therefore, the effects of D_1 and D_m on the isolation between the antenna elements are investigated and depicted in Figs. 7(a) and 7(b). The isolation characteristics are obtained by exciting port 3, as indicated in Fig. 1(b). From Fig. 7(a), it is perceived that as D_1 is increased, S32 and S34 are improving thus indicating better isolation between the adjacent side-by-side elements. Fig. 7(b) highlights that as D_m is increased, S37, S38 and S39 are improving thereby indicating improved isolation between adjacent elements oriented in face-to-face and diagonal directions wherein more prominent improvement is observed for elements in face-to-face orientation.

B. CO-POL TO X-POL ISOLATION IMPROVEMENT

Referring to Fig. 1(d), a defected metal structure is used at the backside of the MIMO antenna for XPR reduction which eventually leads to the improvement of co-pol to X-pol isolation. Fig. 8(a) illustrates the comparison of the

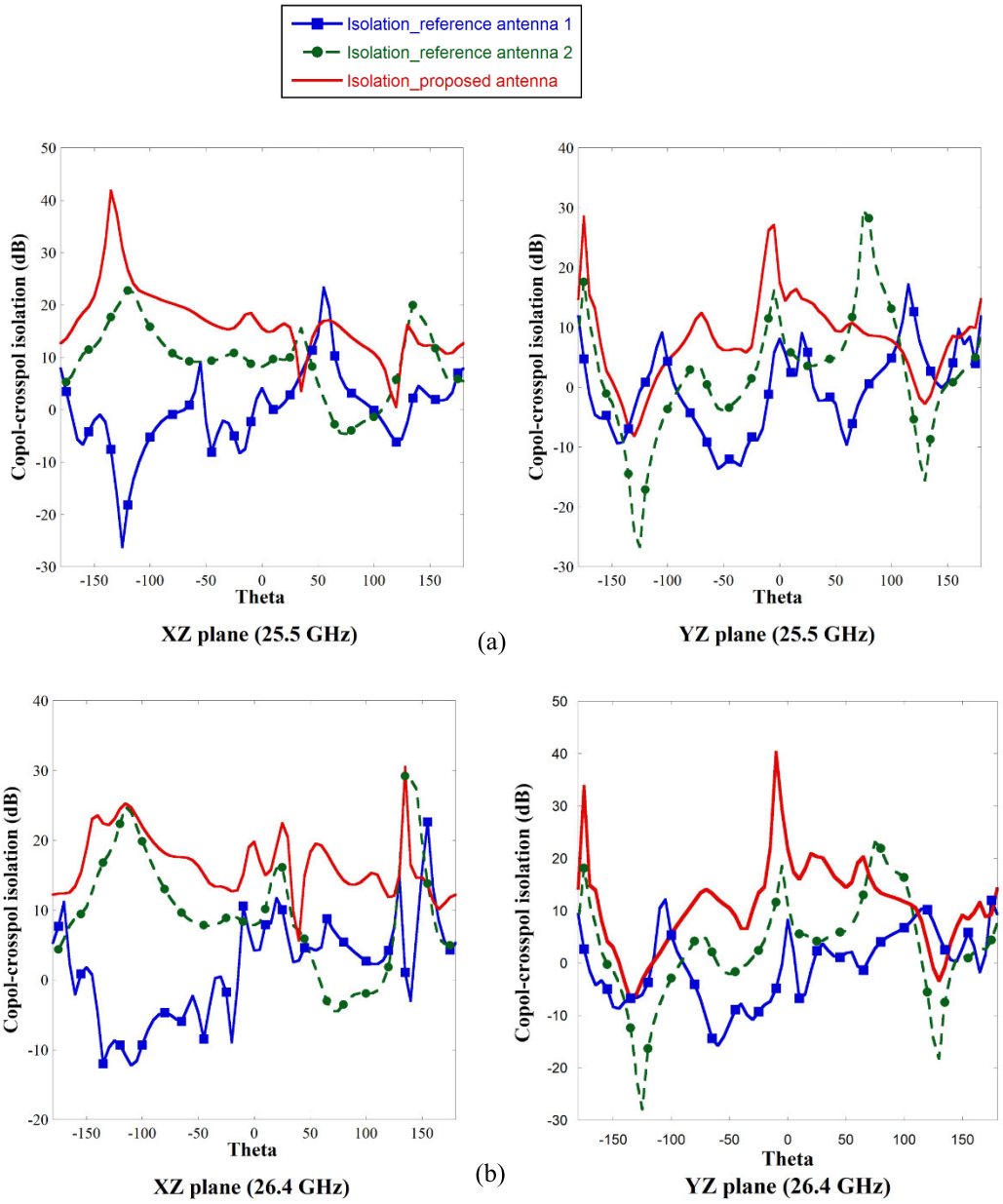

FIGURE 10. co-pol to X-pol isolation graph for XZ plane and YZ plane radiation at (a) 25.5 GHz and (b) at 26.4 GHz of 10-elements MIMO antenna without DGS and DMS (reference antenna1), 10-elements MIMO antenna with DGS (reference antenna2) and 10-elements MIMO antenna with DGS and DMS (proposed antenna).

isolation characteristic between the MIMO structure without DMS but with DGS and the proposed structure with DGS and DMS. It shows that although the mutual coupling has slightly increased on addition of DMS, mainly for side-by-side and face-to-face elements, it is still below −35 dB over the entire operating range which is significantly lower than the MIMO structure without the DGS and DMS. Fig. 8(b) presents the measured isolation characteristic of the fabricated prototype which closely resembles the response of the simulated structure.

The radiation patterns of the proposed MIMO antenna are obtained by exciting the port 3 whereas other ports are connected to 50-ohm matched load. The normalized radiation patterns in XZ ($\varphi = 0°$) and YZ ($\varphi = 90°$) planes are shown in Figs. 9(a) and 9(b) for 25.5 and 26.4 GHz respectively which compare the patterns of the reference antenna 1 (refer to Fig. 1(b)) and reference antenna 2 (refer to Fig. 1(c)) with the proposed structure (refer to Fig. 1(d)) to highlight the reduction in XPR with the addition of DGS and DMS. The figures show that at both the frequencies, the XPR has reduced significantly throughout all the elevation angles (−180° to 180°) at both XZ and YZ planes. In addition to that, the co-pol radiation has also improved, particularly in the vicinity of the boresight direction. The co-pol to X-pol isolation graphs is given in Figs. 10(a) and 10(b) for 25.5 and 26.4 GHz respectively. The figures indicate that, for both the

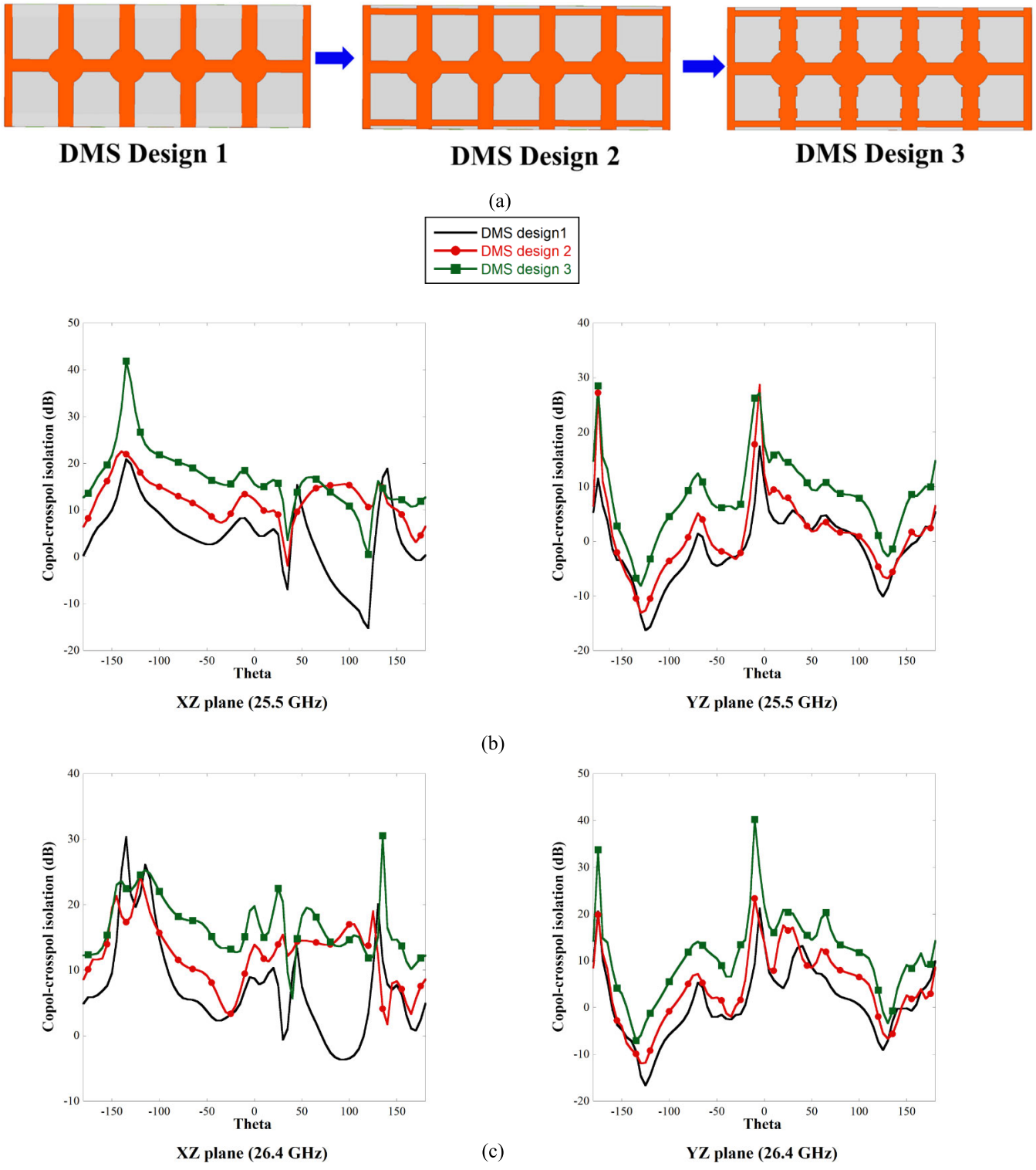

FIGURE 11. (a) Design evolution of the DMS structure, co-pol to X-pol isolation graph for XZ plane and YZ plane radiation according to the design evolution of DMS structure at (b) 25.5 GHz and (c) at 26.4 GHz of 10-elements MIMO.

frequencies, the improved co-pol to X-pol isolation for XZ and YZ planes is above 20 dB and 28 dB at the bore-sight direction respectively. Furthermore, the isolation is maintained above 15 dB over most of the angular range of θ ($-180°$ to $180°$) whereas in case of the reference antenna 1 and reference antenna 2, this isolation is predominantly much below 8 dB which highlights the utility of the DGS and DMS structure to improve the co-pol-to-X-pol isolation. The

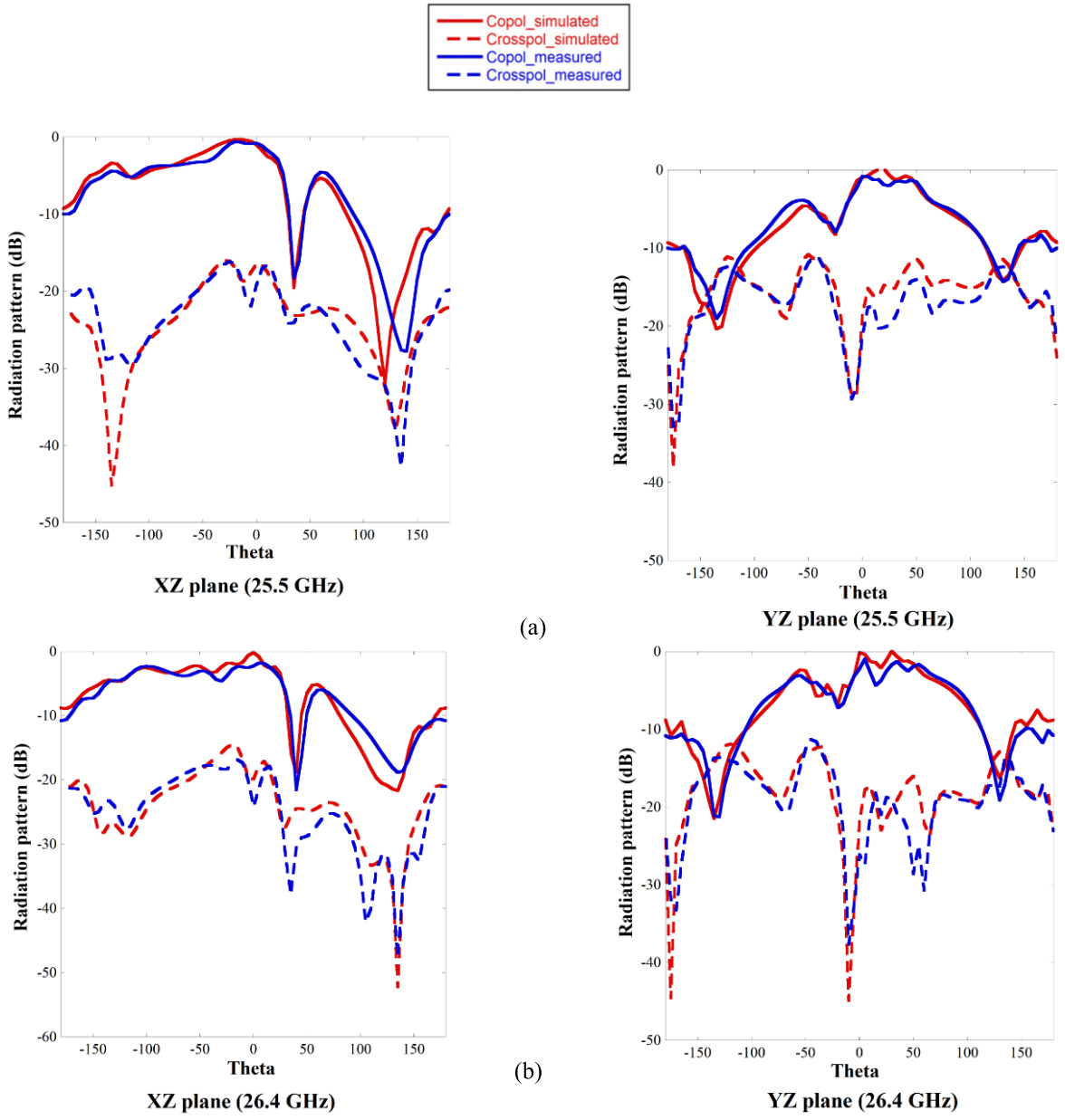

FIGURE 12. Simulated and measured graph of XZ plane and YZ plane radiation pattern in rectangular form at (a) 25.5 GHz and (b) 26.4 GHz of 10-elements MIMO.

step-by-step evolution of the DMS is presented in Fig. 11(a). Fig. 11(b) and 11(c) demonstrate that as the design evolves from step 1 to step 3, the co-pol to X-pol isolation has steadily improved almost throughout the entire elevation angles.

The radiation patterns are measured for the fabricated prototype and compared with simulated results at both the frequencies which are portrayed in Fig. 12 and Fig 13 which show closely similar patterns. It is to be noted that the co-pol radiation patterns are very similar in nature at both the frequencies. Hence, it may be inferred that the radiation patterns remain almost intact within the operating frequency.

Fig. 12 shows the rectangular plot of the radiation pattern whereas Fig. 13 represents the same plot in polar form to visualize the radiation characteristics in practical scenario. The 3D polar plot of the radiation is depicted in Fig. 14 which is portrays the total gain pattern for a port of the proposed MIMO antenna.

High XPR occurs due to strong orthogonal electric field at the non-radiating edge of the antenna [23]. In MIMO antenna the high orthogonal electric field induced between the interelement spaces is also responsible for high XPR. Fig. 15 (a) illustrates the electric field distribution of the reference MIMO antenna 1 (refer to Fig. 1(b)), where strong orthogonal electric fields are noticed near the feedline as well as interelement spaces between the antenna elements of the proposed MIMO structure. In Fig. 15 (b), presents the

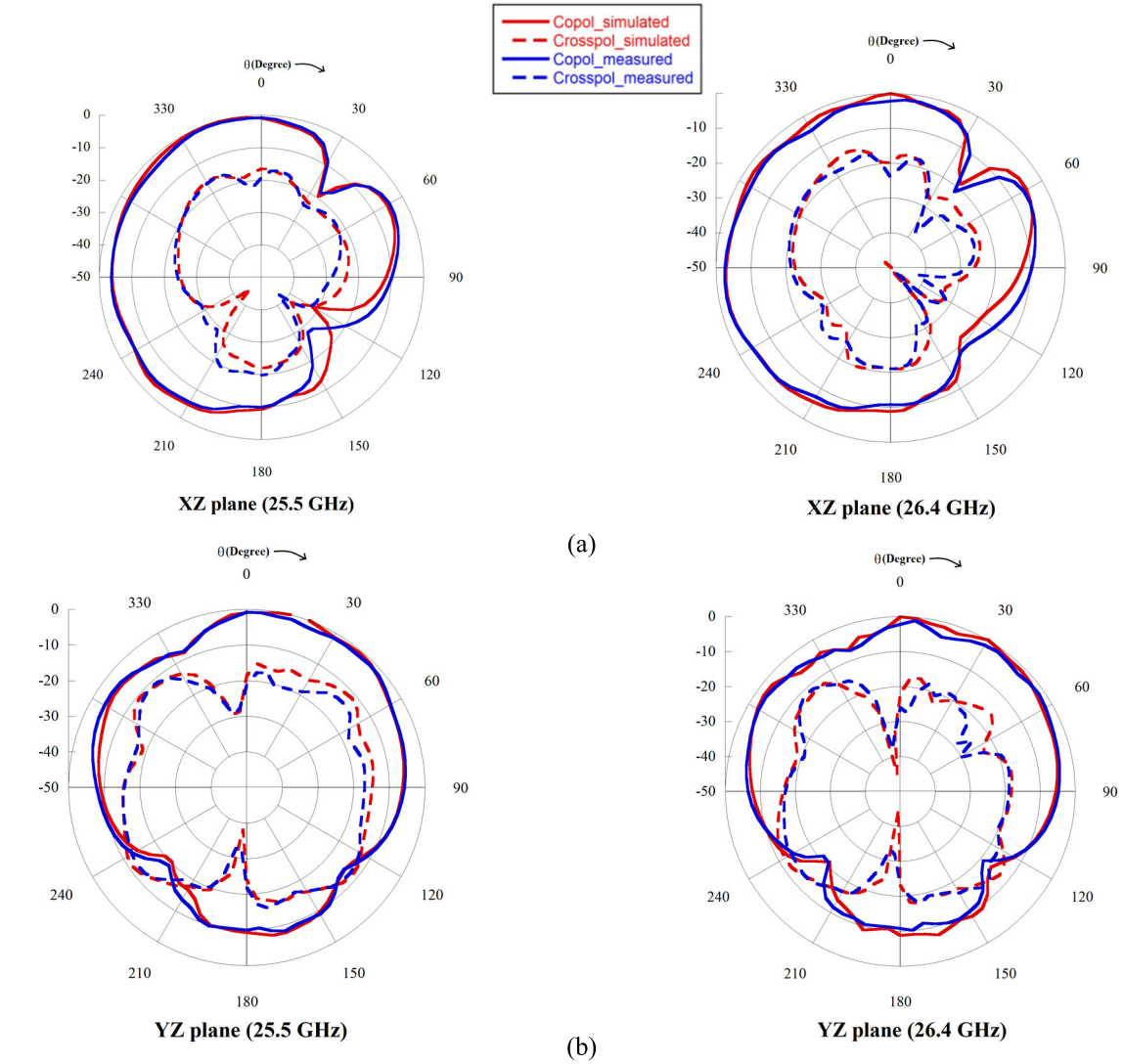

FIGURE 13. Simulated and measured graph of XZ plane and YZ plane radiation pattern in polar form at (a) 25.5 GHz and (b) 26.4 GHz of 10-elements MIMO.

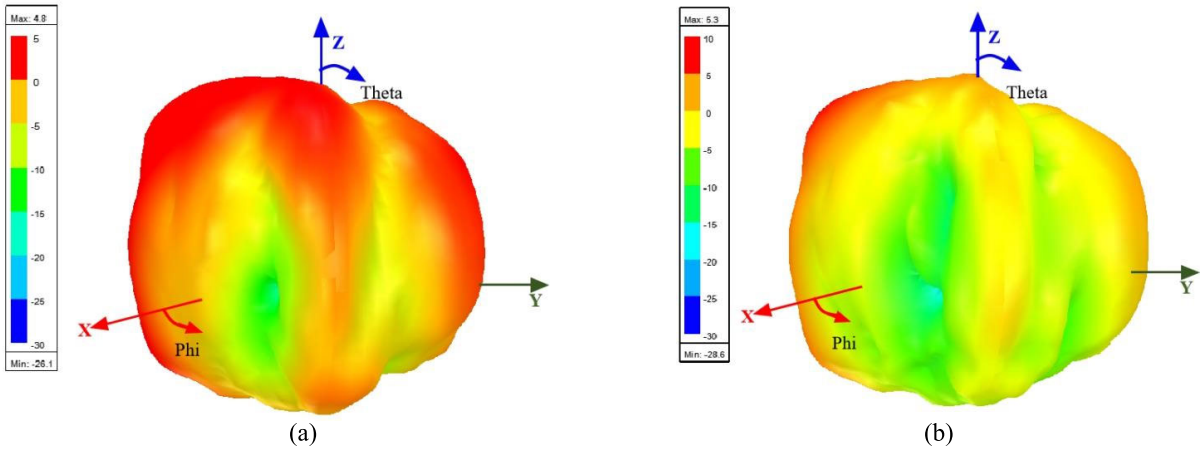

FIGURE 14. 3D polar plot of the gain pattern at (a) 25.5 GHz and (b) 26.4 GHz of 10-elements MIMO.

orthogonal electric field of the reference MIMO antenna 2 (refer to Fig. 1(c)) in the presence of DGS structure, which are not very strong but still present near the feed line of the MIMO antenna. The electric field distribution after the

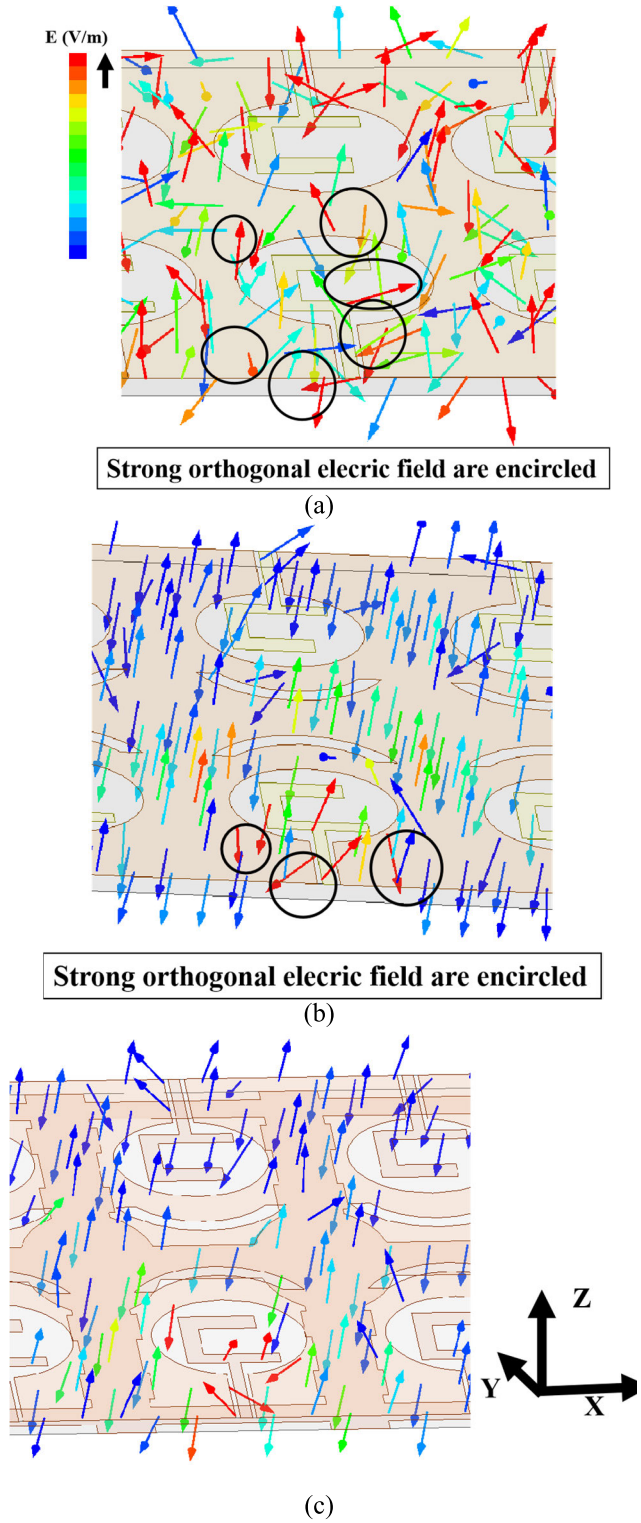

FIGURE 15. Electric field distribution of 10-elements MIMO antenna (a) without DGS and DMS, (b) with DGS and (c) with DGS and DMS.

incorporation of DMS structure (refer to Fig. 1(d)) is presented in Fig. 15 (c). From the figure, it is observed that the DMS structure neutralizes the extra electric field at edges and weaken the orthogonal electric field, therefore having almost no orthogonal electric field component. Hence, XPR

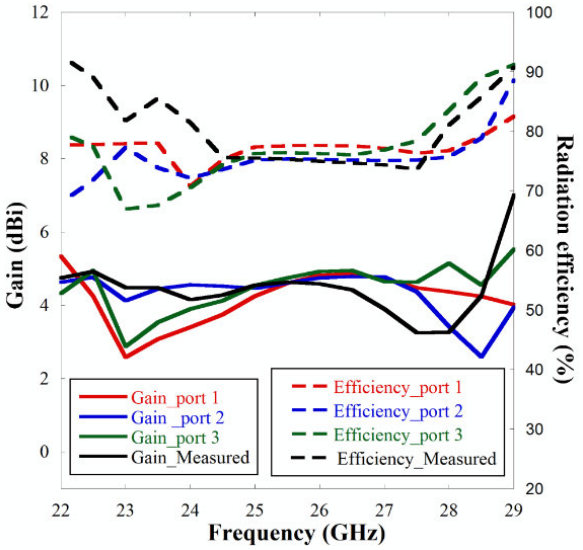

FIGURE 16. Simulated and measured graph of gain and radiation efficiency of proposed 10-elements MIMO antenna with DGS and DMS.

is reduced that eventually improves the co-pol to X-pol isolation.

The gain and radiation efficiency of the proposed 10-elements MIMO structure are obtained by exciting ports 1, 2 and 3 separately. Other ports are not excited because any other port will be symmetric to either port 1, 2 or 3. The gain varies between 2.2-5.3 dBi and the value of radiation efficiency is approximately 77% over the operating bandwidth as shown in Fig. 16. It is observed from the figure that the values are almost similar for each of the ports. Moreover, a flat response is obtained with respect to gain and efficiency within the targeted 5G band n258 (24.25 GHz-27.5 GHz). During measurement, excitation at port 3 is used and the measured results are given in Fig. 16 which confirm the simulated responses.

IV. DIVERSITY PERFORMANCES

The diversity performances are investigated to realize the overall functionality of the 10-elements MIMO antenna in practical MIMO communication system. The diversity performances in terms of ECC, CCL and MEG are calculated using scattering parameters obtained for the MIMO antenna. The diversity performances are calculated for all the possible adjacent orientations of the MIMO antenna elements, that is, side-by-side, face-to-face and diagonal. The ECC value expresses the correlation between adjacent antenna elements as given in Eq. 1 [16],

$$\rho_{ij} = \frac{\left|S_{ii}S_{ij} + S_{ji}S_{jj}\right|^2}{\left(1 - |S_{ii}|^2 - |S_{ij}^2|\right)\left(1 - |S_{jj}|^2 - |S_{ji}^2|\right)} \quad (1)$$

The ECC graph of the proposed structure is presented in Fig. 17 (a) and the maximum value is < 0.003 which is considerably very low and encompasses near zero value within most of the operating bandwidth. This low value indicates that

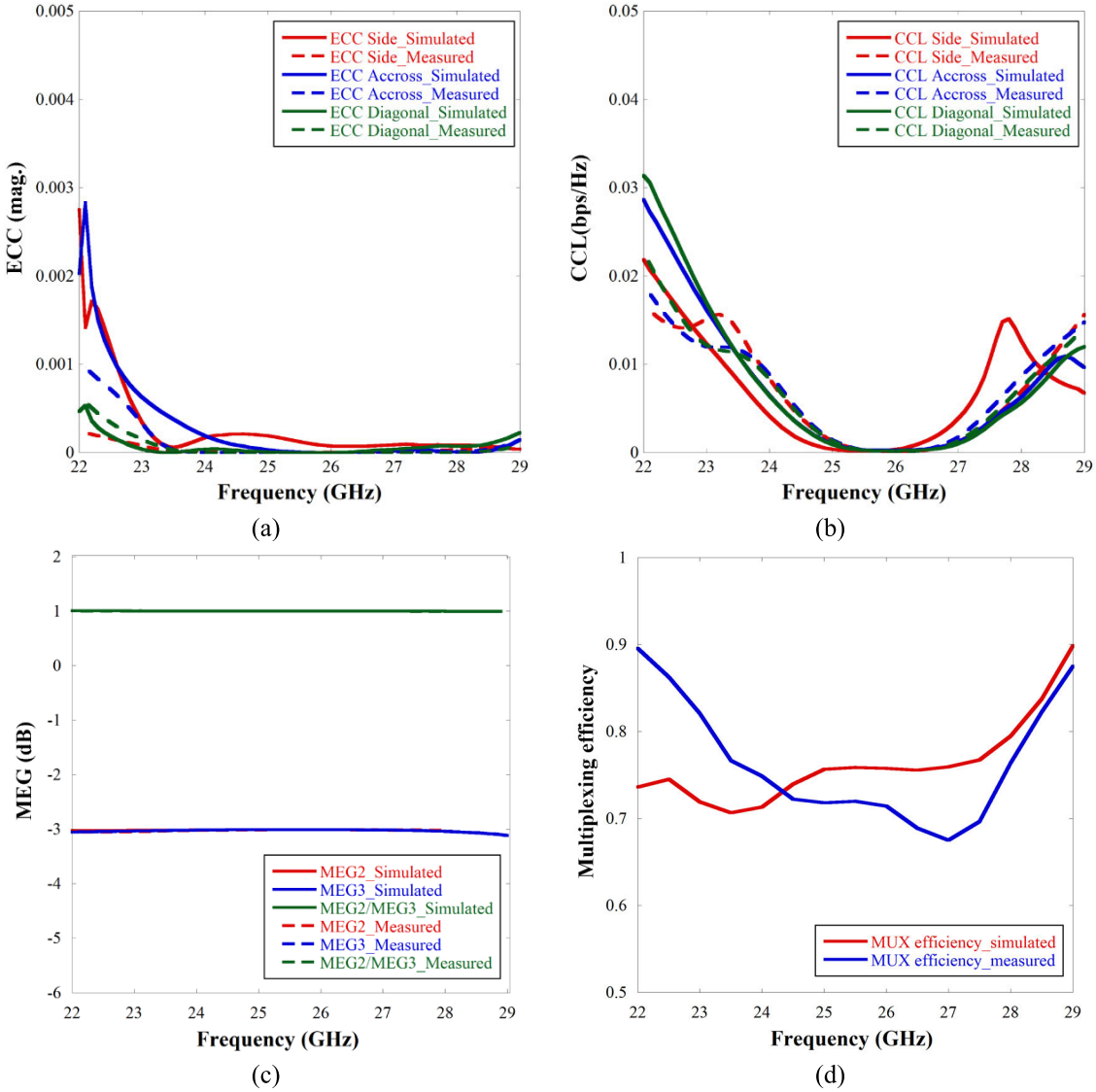

FIGURE 17. (a) Envelop correlation coefficient (ECC), (b) Channel capacity loss (CCL), (c) Mean effective gain (MEG) graph and (d) Multiplexing efficiency of proposed 10-elements MIMO antenna with DGS and DMS.

the MIMO channels will be almost uncorrelated in practical MIMO communication systems for the 10-elements MIMO antenna. The diversity gain is obtained from ECC using Eq. 2 [16] and the value is almost 10 dB which is considered as desired diversity gain for any MIMO antenna [17],

$$\mathrm{DG} = 10\sqrt{1 - |ECC|^2} \tag{2}$$

The channel capacity loss is given by [17],

$$\mathrm{CCL} = -\log_2 \det(S) \tag{3}$$

where,

$$S = \begin{pmatrix} \sigma_{11} & \sigma_{12} \\ \sigma_{21} & \sigma_{22} \end{pmatrix}, \tag{4}$$

$$\sigma_{ii} = 1 - (|S_{ii}|^2 + |S_{ij}|^2), \tag{5}$$

$$\sigma_{ij} = S_{ii}^* S_{ij} + S_{ii} S_{jj}^*) \tag{6}$$

The maximum value of CCL is 0.03 bps/Hz and it is below 0.005 bps/Hz over the operating band as shown in Fig. 17 (b) which implies that extremely low loss data transmission is possible using the proposed MIMO antenna. The MEG is given as [7],

$$MEG_i = 0.5(1 - \sum_{j=1}^{M} |S_{ij}|^2) \tag{7}$$

The MEG is calculated with respect to ports 2 and 3 since they are having the least isolation and is graphically presented in Fig. 17 (c) which shows almost identical response for the ports and the value is less than -3 dB. Due to identical nature of MEG for each port, the ratio of MEG between these two ports is almost 1 as shown in the figure. This MEG response ascertains that the antenna elements are identical with low loss in diversity performance which is a promising advantage for multipath fading scenario.

The multiplexing efficiencies are calculated for port 2 and port 3 which are having least isolation as mentioned before. The multiplexing efficiency includes total efficiency at the individual ports as well as the correlation between them which is measured by [16],

$$\eta MUX_{ij} = \sqrt{\eta_i \eta_j (1 - \rho_{ij})} \tag{8}$$

Here, η_i *and* η_j are representing total efficiency at i^{th} and j^{th} port and ρ_{ij} is envelop correlation coefficient between the i^{th} and j^{th} port as described in Eq. 1. The multiplexing efficiency are presented in Fig. 17 (d). The value of the multiplexing efficiency over the bandwidth is in between 0.67-0.8 which indicates that, the value of the multiplexing efficiency is satisfactory over the bandwidth, and it is suitable for MIMO applications [31].

V. GROUP DELAY

The group delay is described as the changing rate of the transmission phase along with frequency and the unit referred as time unit. For a MIMO system, the group delay measures the time lagging in between the transmitter and receiver burst of the system [32]. Ideally the group delay between two antennas should be constant or variation should be below 1 ns. The constant group delay indicates the liner transmission characteristic of the antenna structure [33]. For the proposed 10-elements MIMO antenna, the group delay is measured by placing two similar types of MIMO antennas separated by the distance greater than $2D^2/\lambda$ where the antennas operate in the far field region. Here, D denotes the diagonal length of the single element antenna and λ denotes the wavelength corresponding the highest cutoff frequency of the proposed MIMO antenna structure. Fig. 18 (a) illustrates the pictorial overview of the arrangement of the proposed MIMO antenna to obtain the group delay. The group delay characteristic is given Fig. 18 (b). The overall group delay is fairly constant with variation within 1.2 ns that indicates linear transmission characteristic of the antenna.

A comparison table with respect to the different features of the proposed MIMO antenna with existing MIMO antenna design for mm-wave applications is provided in Table 2. The proposed MIMO structure has highest number of elements with least inter-element spacing thus signifying a compact design. The minimum isolation between the antenna elements for the proposed MIMO structure is lower than other reported structures except [10, 20] although [10, 20] have higher inter-element spacing thereby compromising the compactness of the structure. High XPR is a severe problem for a MIMO antenna design. As a result of which the reported structures either have high co-pol to X-pol isolation or not provided any information regarding XPR. The proposed design has implemented a technique to reduce XPR thereby achieving maximum co-pol-to-corsspol isolation among the reported structures. The ECC value of the proposed structure is least among the enlisted literature and same as [20] whereas [20] comprises of only 4 elements with higher inter-element spacing. Thus, the proposed MIMO antenna is advantageous for its superior performance in terms of no. of antenna elements, compactness, isolation, co-pol to X-pol radiation isolation and ECC.

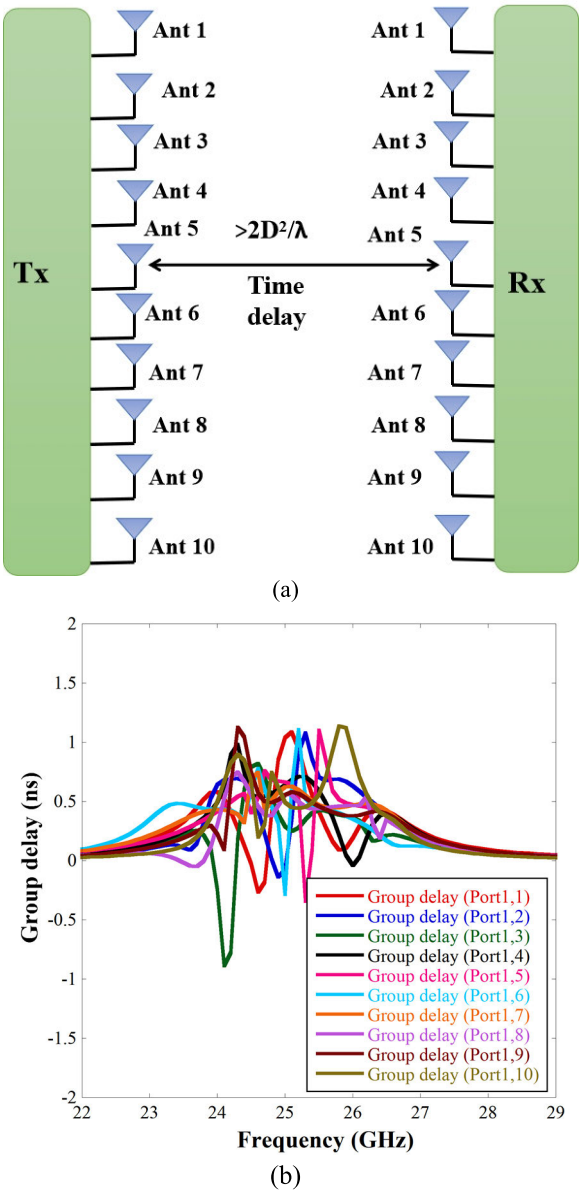

FIGURE 18. (a) The arrangement of the 10-elements MIMO antenna to measure the group delay, (b) Group delay of the 10-elements MIMO antenna.

VI. CONCLUSION

A 10-elements CPW-fed MIMO antenna has been proposed within a compact layout with a bandwidth of 23.52% (22.5GHz-28.5 GHz) which covers the mm-wave 5G frequency band n258 (24.2-27.8 GHz). DGS and DMS structures have been incorporated to improve the inter-element isolation and enhance the co-pol to X-pol radiation isolation respectively thereby achieving high isolation of over 35 dB and co-pol to X-pol radiation isolation of more than 20 dB

and 28 dB in the boresight direction at XZ and YZ planes respectively. The design evolution study of the DMS structure has been investigated and improvement steps of the radiation characteristics are reported accordingly. The diversity performances have been examined in terms of ECC, CCL, MEG and Multiplexing efficiency which confirm that the antenna is suitable for low-loss and high data transmission MIMO systems. The time-domain characteristic of proposed structure has been investigated through group delay analysis with satisfactory results. All the antenna parameters have been validated by experimental results thus confirming that the proposed antenna is a potential candidate to be used in 5G mm-wave MIMO communication systems.

REFERENCES

[1] O. Jo, J.-J. Kim, J. Yoon, D. Choi, and W. Hong, "Exploitation of dual-polarization diversity for 5G millimeter-wave MIMO beamforming systems," *IEEE Trans. Antennas Propag.*, vol. 65, no. 12, pp. 6646–6655, Dec. 2017.

[2] A. Khabba, J. Amadid, S. Mohapatra, Z. El Ouadi, S. Ahmad, S. Ibnyaich, and A. Zeroual, "UWB dual-port self-decoupled o-shaped monopole MIMO antenna with small-size easily extendable design and high diversity performance for millimeter-wave 5G applications," *Appl. Phys. A, Solids Surf.*, vol. 128, no. 8, pp. 1–23, Aug. 2022.

[3] I. E. Lamri, S. Ahmad, E. M. A. R. Ali, M. Belattar, M. Dalarsson, and M. Alibakhshikenari, "Four-elements proximity coupled MIMO antenna for mm-wave 5G applications," in *Proc. Int. Workshop Antenna Technol. (iWAT)*, May 2022, pp. 188–191.

[4] H. Qiu, H. Liu, X. Jia, Z-Y Jiang, Y.-H. Liu, J. Xu, T. Lu, M Shao, T.-L. Ren, and K. J. Chen, "Compact, flexible, and transparent antennas based on embedded metallic mesh for wearable devices in 5G wireless network," *IEEE Trans. Antennas Propag.*, vol. 69, no. 4, pp. 1864–1873, Apr. 2021.

[5] S. F. Jilani and A. Alomainy, "Millimetre-wave T-shaped MIMO antenna with defected ground structures for 5G cellular networks," *IET Microw., Antennas Propag.*, vol. 12, no. 5, pp. 672–677, Apr. 2018.

[6] D. A. Sehrai, M. Asif, W. A. Shah, J. Khan, I. Ullah, M. Ibrar, S. Jan, M. Alibakhshikenari, F. Falcone, and E. Limiti, "Metasurface-based wideband MIMO antenna for 5G millimeter-wave systems," *IEEE Access*, vol. 9, pp. 125348–125357, 2021.

[7] M. Bilal, S. I. Naqvi, N. Hussain, Y. Amin, and N. Kim, "High-isolation MIMO antenna for 5G millimeter-wave communication systems," *Electronics*, vol. 11, no. 6, p. 962, Mar. 2022.

[8] M. Hussain, E. Mousa Ali, S. M. R. Jarchavi, A. Zaidi, A. I. Najam, A. A. Alotaibi, A. Althobaiti, and S. S. M. Ghoneim, "Design and characterization of compact broadband antenna and its MIMO configuration for 28 GHz 5G applications," *Electronics*, vol. 11, no. 4, p. 523, Feb. 2022.

[9] A. Desai, C. D. J. Bui Patel, T. Upadhyaya, G. Byun, and T. K. Nguyen, "Compact wideband four element optically transparent MIMO antenna for mm-wave 5G applications," *IEEE Access*, vol. 8, pp. 195206–195217, 2020.

[10] A. Patel, A. Desai, I. Elfergani, A. Vala, H. Mewada, K. Mahant, S. Patel, C. Zebiri, J. Rodriguez, and E. Ali, "UWB CPW fed 4-port connected ground MIMO antenna for sub-millimeter-wave 5G applications," *Alexandria Eng. J.*, vol. 61, no. 9, pp. 6645–6658, Sep. 2022.

[11] Y. S. Faouri, S. Ahmad, N. O. Parchin, C. H. See, and R. Abd-Alhameed, "A novel meander bowtie-shaped antenna with multi-resonant and rejection bands for modern 5G communications," *Electronics*, vol. 11, no. 5, p. 821, Mar. 2022.

[12] S. Sharma and M. Arora, "A millimeter wave elliptical slot circular patch MIMO antenna for future 5G mobile communication networks," *Prog. Electromagn. Res. M*, vol. 110, pp. 235–247, 2022.

[13] H.-C. Huang and J. Lu, "Evolution of innovative 5G millimeter-wave antenna designs integrating non-millimeter-wave antenna functions based on antenna-in-package (AiP) solution to cellular phones," *IEEE Access*, vol. 9, pp. 72516–72523, 2021.

[14] J. Acharjee, K. Mandal, and S. K. Mandal, "Reduction of mutual coupling and cross-polarization of a MIMO/diversity antenna using a string of H-shaped DGS," *AEU Int. J. Electron. Commun.*, vol. 97, pp. 110–119, Dec. 2018.

[15] F. El Moukhtafi, M. Aoutoul, K. Sabri, A. Sarosh, A. Khoukh, Y. Errami, R. Jouali, A. Haddad, and A. Had, "A planar patch antenna array design with reduced mutual coupling using a novel absorber," *Arabian J. Sci. Eng.*, 2022, doi: 10.1007/s13369-022-07148-y.

[16] A. Iqbal, O. A. Saraereh, A. W. Ahmad, and S. Bashir, "Mutual coupling reduction using F-shaped stubs in UWB-MIMO antenna," *IEEE Access*, vol. 6, pp. 2755–2759, 2018.

[17] A. Khan, S. Bashir, S. Ghafoor, and K. K. Qureshi, "Mutual coupling reduction using ground stub and EBG in a compact wideband MIMO-antenna," *IEEE Access*, vol. 9, pp. 40972–40979, 2021.

[18] I. Adam, M. N. M. Yasin, N. Ramli, M. Jusoh, H. A. Rahim, T. B. A. Latef, T. F. T. M. N. Izam, and T. Sabapathy, "Mutual coupling reduction of a wideband circularly polarized microstrip MIMO antenna," *IEEE Access*, vol. 7, pp. 97838–97845, 2019.

[19] M. Farahani, J. Pourahmadazar, M. Akbari, M. Nedil, A. R. Sebak, and T. A. Denidni, "Mutual coupling reduction in millimeter-wave MIMO antenna array using a metamaterial polarization-rotator wall," *IEEE Antennas Wireless Propag. Lett.*, vol. 16, pp. 2324–2327, 2017.

[20] S. Tariq, S. I. Naqvi, N. Hussain, and Y. Amin, "A metasurface-based MIMO antenna for 5G millimeter-wave applications," *IEEE Access*, vol. 9, pp. 51805–51817, 2021.

[21] S. Gupta, Z. Briqech, A. R. Sebak, and T. A. Denidni, "Mutual-coupling reduction using metasurface corrugations for 28 GHz MIMO applications," *IEEE Antennas Wireless Propag. Lett.*, vol. 16, pp. 2763–2766, 2017.

[22] D. Guha, M. Biswas, and Y. M. M. Antar, "Microstrip patch antenna with defected ground structure for X-polarization suppression," *IEEE Antennas Wireless Propag. Lett.*, vol. 4, pp. 455–458, 2005.

[23] D. Guha, C. Kumar, and S. Pal, "Improved cross-polarization characteristics of circular microstrip antenna employing arc-shaped defected ground structure (DGS)," *IEEE Antennas Wireless Propag. Lett.*, vol. 8, pp. 1367–1369, 2009.

[24] R. Dehdasht-Heydari and M. Naser-Moghadasi, "Introduction of a novel technique for the reduction of cross polarization of rectangular microstrip patch antenna with elliptical DGS," *J. Electromagn. Waves Appl.*, vol. 22, nos. 8–9, pp. 1214–1222, Jan. 2008.

[25] D. Ghosh, S. K. Ghosh, S. Chattopadhyay, S. Nandi, D. Chakraborty, R. Anand, R. Raj, and A. Ghosh, "Physical and quantitative analysis of compact rectangular microstrip antenna with shorted non-radiating edges for reduced cross-polarized radiation using modifi ed cavity model," *IEEE Antennas Propag. Mag.*, vol. 56, no. 4, pp. 61–72, Aug. 2014.

[26] N.-W. Liu, L. Zhu, Z.-X. Liu, Z.-Y. Zhang, G. Fu, and Y. Liu, "Cross-polarization reduction of a shorted patch antenna with broadside radiation using a pair of open-ended stubs," *IEEE Trans. Antennas Propag.*, vol. 68, no. 1, pp. 13–20, Jan. 2020.

[27] S. H. Zhu, X.-S. Yang, J. Wang, N.-S. Nie, and B.-Z. Wang, "Mutual coupling reduction of ±45° dual-polarized closely spaced MIMO antenna by topology optimization," *IEEE Access*, vol. 8, pp. 29089–29098, 2020.

[28] M. Xue, W. Wan, Q. Wang, and L. Cao, "Low-profile millimeter-wave broadband metasurface antenna with four resonances," *IEEE Antennas Wireless Propag. Lett.*, vol. 20, no. 4, pp. 463–467, Apr. 2021.

[29] M. Alzidani, I. Afifi, M. Asaadi, and A.-R. Sebak, "Ultra-wideband differential fed hybrid antenna with high-cross polarization discrimination for millimeter wave applications," *IEEE Access*, vol. 8, pp. 80673–80683, 2020.

[30] M. Khalily, R. Tafazolli, P. Xiao, and A. A. Kishk, "Broadband mm-wave Microstrip array antenna with improved radiation characteristics for different 5G applications," *IEEE Trans. Antennas Propag.*, vol. 66, no. 9, pp. 4641–4647, Sep. 2018.

[31] S. Nej, A. Ghosh, S. Ahmad, A. Ghaffar, and M. Hussein, "Compact quad band MIMO antenna design with enhanced gain for wireless communications," *Sensors*, vol. 22, no. 19, p. 7143, Sep. 2022.

[32] S. Ahmad, S. Khan, B. Manzoor, M. Soruri, M. Alibakhshikenari, M. Dalarsson, and F. Falcone, "A compact CPW-fed ultra-wideband multi-input-multi-output (MIMO) antenna for wireless communication networks," *IEEE Access*, vol. 10, pp. 25278–25289, 2022.

[33] A. Ghosh, T. Mandal, and S. Das, "Design and analysis of triple notch ultrawideband antenna using single slotted electromagnetic bandgap inspired structure," *J. Electromagn. Waves Appl.*, vol. 33, no. 11, pp. 1391–1405, Jul. 2019.

SANJUKTA NEJ was born in Burdwan, West Bengal, India, in 1994. She received the B.E. degree in electronics and communication engineering from the University Institute of Technology, Burdwan University, West Bengal, in 2015, and the M.Tech. degree in electronics and communication engineering (specialization in microwave engineering) from Burdwan University, in 2017. Currently, she is pursuing the Ph.D. degree with the Department of Electronics and Communication Engineering, National Institute of Technology, Mizoram, India. Her research interests include antennas, MIMO systems, and frequency selective surfaces.

ANUMOY GHOSH was born in 1987. He received the B.Tech. degree in electronics and communication engineering from Kalyani Government Engineering College, West Bengal University of Technology, India, in 2010, the M.E. degree from Bengal Engineering and Science University, Shibpur, India, in 2012, and the Ph.D. degree from the Indian Institute of Engineering Science and Technology, India, in 2018. Since 2014, he has been an Assistant Professor with the Department of Electronics and Communication Engineering, National Institute of Technology, Mizoram, India. His current research interests include planar antennas, periodic structures RFID systems, and RF energy harvesting.

SAROSH AHMAD (Graduate Student Member, IEEE) received the bachelor's degree in electrical engineering with specialization in telecommunication from the Department of Electrical Engineering and Technology, Government College University Faisalabad (GCUF), Pakistan, in 2021. He is currently pursuing the master's degree in advanced communication technology with the Department of Signal Theory and Communications, Universidad Carlos III de Madrid (UC3M), Madrid, Spain. He has published 18 conference papers, 35 high indexed international journals, and seven book chapters by Springer. His research interests include antennas and propagations, rectennas for energy harvesting applications, bandpass filters, half- and full-wave filter antennas, active sensors, and the microwave imagining communication devices. He is a member of the IEEE Antennas and Propagation Society (APS). He received the Fully Funded PEEF Scholarship Award from the Prime Minister of Pakistan and the Silver Medal for his bachelor's program and the Fully Funded Erasmus Grant Scholarship for his master's program in Madrid. He was a Branch Treasurer at the IEEE GCUF, Faisalabad Subsection, for two years. During his graduation research period, he has participated in four international IEEE conferences over the world, where he has presented ten articles mostly in oral presentations. He has presented his two articles in the International Turkish Conferences, where he has got the Best Paper Award, one article in the International Moroccan Conference Proceedings and one article in IEEE EuCAP'22. He has served the 16th IEEE European Conferences on Antennas and Propagations as a Volunteer. He has been selected for the fully funded MITACS Internship Program in the nationally ranked University of Canada called Carleton University, where he is working as a Researcher in the field of massive MIMO antennas.

JAYENDRA KUMAR (Senior Member, IEEE) received the B.E. and M.E. degrees from Solapur University, Maharashtra, India, in 2011 and 2014, respectively, and the Ph.D. degree from the National Institute of Technology Silchar, Assam, India, in 2018. He was working on electronic bandgap structures (EBGs), ultra-wideband antennas, and mutual coupling reduction in multiple-input multiple-output (MIMO) antennas. He is currently an Associate Professor with the Department of Electronics and Communication Engineering, Vellore Institute of Technology, Amaravati. He is currently with the frequency reconfigurable, reduced surface waves (RSWs), and high gain single element antennas. His research interests include dielectric resonator antennas, metamaterials/metasurface, conformal antennas, multilayered substrates, and higher-order modes antennas. He has delivered guest lectures and short-term training programs (STTPs) on microstrip antennas, high-frequency structural simulators (HFSS), MATLAB, and solar energy awareness programs. He is a member of IEEE Antennas and waves Propagation Society (APS), IEEE Microwave Theory and Techniques Society, and the Lifetime Indian Society of Technical Education (ISTE). He is a Reviewer of IEEE TRANSACTION ON VEHICULAR TECHNOLOGY, *IEEE Communication Magazine*, *International Journal of systems, control and communications* (IJSCC), *AEU-International Journal of Electronics and Communications*, *SN Applied Sciences*, and *Computer and Electrical Engineering Journal*.

ADNAN GHAFFAR received the B.Sc. degree in computer engineering from BZU Multan, Pakistan, in 2010, and the M.E. degree in circuits and systems from Lanzhou Jiaotong University, Lanzhou, China, in 2015. He is currently pursuing the Ph.D. degree in electrical and electronics engineering with the Auckland University of Technology, Auckland, New Zealand. His research interests include RF circuits, reconfigurable antenna, embedded systems, metasurface antenna, flexible, and wearable antenna design.

MOUSA I. HUSSEIN (Senior Member, IEEE) received the B.Sc. degree from West Virginia Tech, USA, in 1985, and the M.Sc. and Ph.D. degrees from the University of Manitoba, Winnipeg, MB, Canada, in 1992 and 1995, respectively, all in electrical engineering. From 1995 to 1997, he was with the Research and Development Group, Integrated Engineering Software Inc., Winnipeg, working on developing EM specialized software based on the boundary element method. In 1997, he joined as an Assistant Professor at the Faculty of Engineering, Amman University, Amman, Jordan. He is currently a Professor with the Electrical Engineering Department, United Arab Emirates University. He has over 70 publications in international journals and conferences. He has supervised several Ph.D. and M.Sc. students. His current research interests include computational electromagnetics, electromagnetic scattering, antenna analysis and design, metamaterial and applications, material/bio-material characterization, and sensor design for bio applications.